









Research Article

A Novel High-Efficiency Multiple Output Single Input Step-Up Converter with Integration of Luo Network for Electric Vehicle Applications

Senthil Kumar Ramu ¹, Rajesh Kumar Balaganesh ²,
Suresh Kalichikadu Paramasivam ¹, Suresh Muthusamy ³, Hitesh Panchal ⁴,
Ramakrishna S. S. Nuvvula ⁵, Polamarasetty P Kumar ⁵ and Baseem Khan ⁶

¹Department of Electrical and Electronics Engineering, Sri Krishna College of Technology (Autonomous), Coimbatore, Tamil Nadu, India

²Department of Electrical and Electronics Engineering, M.Kumarasamy College of Engineering (Autonomous), Karur, Tamil Nadu, India

³Department of Electronics and Communication Engineering, Kongu Engineering College (Autonomous), Perundurai, Erode, Tamil Nadu, India

⁴Department of Mechanical Engineering, Government Engineering College, Patan, Gujarat, India

⁵Department of Electrical and Electronics Engineering, GMR Institute of Technology, Rajam 530049, India

⁶Department of Electrical and Computer Engineering, Hawassa University, Hawassa, Ethiopia

Correspondence should be addressed to Baseem Khan; baseem_khan04@yahoo.com

Received 16 June 2022; Accepted 25 July 2022; Published 5 September 2022

Academic Editor: Indragandhi v

Copyright © 2022 Senthil Kumar Ramu et al. This is an open access article distributed under the Creative Commons Attribution License, which permits unrestricted use, distribution, and reproduction in any medium, provided the original work is properly cited.

Concerns about pollution, climate change, limited fossil fuel supplies, and the desire to eliminate energy dependency have sparked a surge in interest in electric vehicles (EVs). EV requirements have resulted in a variety of difficulties and remedies in EV technology. One of them is the use of DC-DC converters to transfer the level of voltage from the battery in an EV to other needed voltage levels. An independent converter for each operating voltage might be used as a remedy. On the other hand, single input multiple output (SIMO) converters can be utilized to decrease costs, reduce switching loss, and thus enhance the system efficiency. In this paper, a nonisolated step-up converter with the integration of the Luo network is proposed for multiple outputs (24 V and 48 V). In electric vehicles, 48 V is utilized for battery backup, while 24 V is utilized for the horns, headlights, telematics, or the microcontroller. The experimental observations of a 36 V, 600 mA, 24 W prototype confirm the theoretic examination and demonstrate the advantages of the proposed converter over other multioutput converters. The STM microcontroller, based on an ARM cortex microprocessor, is linked into the Luo network for making pulses. The proposed converter achieves 94.2% efficiency at full power. The proposed converter's performance is evaluated through MATLAB/SIMULINK software, and the results are validated experimentally.

1. Introduction

Because of looming pollution, finite fossil fuel supplies, the cost of fuel, and stringent environmental rules, the need for environmentally friendly transportation solutions has been exploded in recent decades. As a result, electric motor-based

vehicle technologies are quickly increasing to replace the traditional mechanical drive train transportation industry [1, 2]. The boost converter is required because of the uncertainties of photo voltaic (PV) systems, low voltage at the load side, and the charging of EVs or hybrid electric vehicles (HEV) [3].

In general, to meet the demand for varied voltage levels, the numerous single input multiple outputs (SIMOs) with variable voltage gain are coupled. However, the system control is quite complicated, and the associated cost is higher. The goal of this research is to create a SIMO converter that improves efficiency by decreasing design complication and lowering fabrication costs [4]. Isolated SIMO features several winding transformers for accommodating numerous loads. By raising the number of turns of the power converter, the configuration can afford a higher voltage [5]. Moreover, there are substantial downsides, like increased circulation current and an additional phase of diode that is considerably greater than the final voltage [6]. The voltage gain of nonisolated power converters is inherently quite large. Because of the enormous ripple current, the high duty cycle produces a major reverse recovery difficulty and a drop in efficacy [7]. As a result, a nonisolated type with a suitable duty cycle that achieves more efficiency and voltage gain is required [8, 9].

Reference [10] demonstrated a SIMO capable of producing boost and buck output all at the same time. However, more than three switches are required for a single output. This technique is only appropriate for minimum voltage, and power alteration is degraded because of harsh switching action. The multiple output boost converter for high-and low-level applications discussed in ref. [11] can distribute its total output across several series of voltage levels. Furthermore, more than two switches were required for one output, and the control method was difficult. Also, the equivalent output power cannot be independently provided for individual loads. A boosting action of switching with two outputs is intended for PV applications. However, dual outputs necessitate the use of three switches [12]. Reference [13] discussed three outputs with minimal voltage strains on switches for electric vehicles. However, the addition of numerous components has resulted in a complicated circuit, as well as a decrease in efficiency in the aforementioned converter [14]. A flyback converter can be merged with another layout, and voltage gain can be attained by altering the turn ratio of the connected inductor through a linked inductor [15, 16].

The Luo network is a DC-DC converter that reduces ripples while enhancing the voltage gain in solar panel outputs [17]. The boost converter is the most common DC-DC converter for stepping up situations. However, it has certain drawbacks when contrasted with Luo topology. It could enhance the input voltage in an algebraic or geometric way. It has a large voltage gain, the ripple current is low, and it has a high energy density. Luo converters have been more popular in recent years because of their ease of operation and management. An inductor, a capacitor, and two diodes are used in the design of the Luo converter [18]. In Luo converters, a variety of voltage lift mechanisms are employed. The voltage across the output grows in mathematical progression with the voltage lift technique. The voltage lift approach is better at dealing with intrinsic element parameter uncertainty and stability constraints, which enhances the super lift output voltage. The technology outperforms the voltage lift approach and can boost voltage

transfer gain through a variety of methods. The Super-Luo converter is better at increasing voltage in geometric development. The most prevalent type of Luo network is the super lift. There are three sorts of circuits in this family: basic, relift, and triple circuits [19]. Using a Luo topology in conjunction with a standard step-up converter can enhance circuit constraints, decreasing switch strains and increasing the region of operation in conduction mode. Positive Output Super-Lift DC (POSLDC) is one of the methods to get an appropriate step-up ratio. POSLDC converters outperform buck-boost, SEPIC, and boost converters in terms of efficiency, high capacity, voltage control gain, and voltage enhancement. The existence of zero on the right side of the S plane causes a nonminimum phase problem in a number of converters, such as buck boost, boost, and flyback. PID controllers must, therefore, perform satisfactorily in the presence of line disturbance, parametric uncertainty, and load [20]. Hence, the design technique is strictly adhered to eliminate nonminimum phase problems for achieving optimal converter performance.

To enhance voltage gain and efficiency, step-up non-isolated type converters are being explored. The flyback converter is employed in power devices with several outputs as a traditional, isolated-type step-up converter with a low number of parts, simple structure, and low price. Using a linked inductor, a flyback converter can be combined with other topologies [7]. The authors of [21] described a DC-DC converter that could provide buck-boost and extend inversion outputs at the same time. This converter features three switches and is designed for low-power applications. Switches are controlled in hard-switching circumstances in this arrangement. These converters are intended for small power applications and utilize a complicated structure to calculate zero inductor and peak-inductor currents. Conventional boost converters are popular because of their simple form and inexpensive cost, although they create significant input current fluctuations. This converter requires a high duty cycle ratio to get significant voltage gain, which presents switching difficulties. Hence, in this paper, a SIMO converter for step-up applications is anticipated by combining a POSLDC with a flyback scheme. The block diagram of the proposed system is shown in Figure 1. The SIMO converter is developed in this work using a STM32f103c6 controller. The perturb and observe (P&O) approach is used to get the most power out of the solar panel [22]. The P&O technique works by varying the output voltage and measuring the effect on the output power, because the P&O method is simple to implement. The proposed converter can generate 36 V from a 12 V solar panel and power a 40 W LED lamp using the STM controller and the P&O method of maximum power point tracking (MPPT).

The main objective of this paper is to develop a step-up converter with multiple outputs and single inputs based on the POSLDC network for producing nonisolated outputs. The proposed converter achieves dual outputs by combining a POSLDC converter and a linked inductor with a single input. The proposed converter employs a single power switch to achieve higher efficiency in power transmission, a

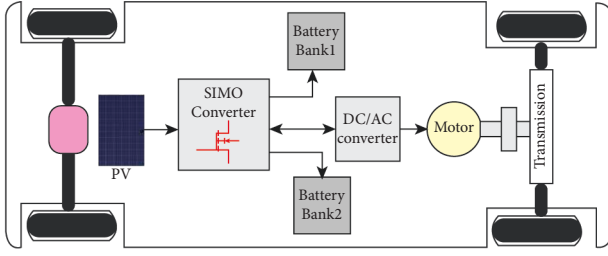


FIGURE 1: Block Diagram of Proposed SIMO Converter in EV.

high step-up rate, and multiple output voltages. Soft switching and voltage clamping techniques are used in the proposed SIMO converter to decrease conduction and switching losses via the use of a minimum power switch.

This paper is structured as follows: section 2 presents the operation of the proposed converter. Section 3 describes the design steps for the proposed converter. Section 4 discusses the results of the proposed system. Section 5 shows a comparison of the observed results to previously published works. Section 6 focuses on the conclusion of the paper.

2. Operation of Proposed Converter

In this paper, a SIMO converter with two separate step-up outputs is developed. Different voltage levels are required by various pieces of equipment in electric vehicles, including the electric motor, audio system, and lighting [23]. As a result, EV is the best application for the newly presented structure. Figure 2 illustrates the circuit diagram of the proposed converter. It is linked to the POSLDC and the flyback network. It provides two outputs through a single switch. As seen in Figure 2, the proposed converter includes a solar-powered input source V_{in} , two linked inductors L_1 and L_2 on one core, diodes D_1 , D_2 , D_3 , and capacitors C_1 , C_2 , C_3 with a switch Q_1 . The converter control system can be implemented using the STM32f103c6 controller. The controller's switching frequency is maintained as a constant. High gain voltages can be generated using this technology with simple structures and no additional transformers or electric circuits for control, regulation, or other purposes. As a result, the resulting output voltage is more energy efficient.

2.1. Mode 1. The mode 1 operation of the proposed converter is shown in Figure 3. The performance of the converter is examined in this section during continuous conduction mode (CCM) circumstances. Using a Luo converter in conjunction with flyback architecture would reduce switch stress while also widening the operational region in CCM. The switching of S_1 , which is regulated by duty cycles D , has an impact on the outputs. Turning on the switch at t_0 initiates this mode, and L_1 , D_1 , and C_2 are the points where the current flows. The voltage across D_1 becomes zero in this state, and it turns on. The magnetizing inductor L_m is energized, and the diodes D_2 and D_3 are reverse biased. The voltage across C_1 gets charged to V_{in} till the turn-on period DT .

The capacitor current can be written as follows:

$$I_{c1} = \frac{V_{in} - V_{c1}}{R_{c1}} e^{-(t-t_0)/\tau}, \quad (1)$$

where $\tau = C_1 R_{c1}$.

In this mode, the C_1 charging current grows exponentially. The charging current's starting value is determined by the initial voltage across C_1 and the switch's impedance. The charging current's maximum amplitude is limited by R_{c1} . The voltage over capacitor C_1 reaches approximately V_{in} at the completion of this mode, and diode D_1 is switched off. The loads are provided by the discharging output capacitors C_1 and C_2 , respectively.

2.2. Mode 2. The mode 1 operation of the proposed converter is illustrated in Figure 4. Switch Q_1 is turned off during the period $(1-D)T$, and inductor current i_{L1} decreases with voltage $V_0 - 2V_{in}$. Because of its forward bias, diodes D_2 and D_3 conduct, and power is delivered to the outputs through the linked inductor L_2 . D_1 is turned off in this mode since D_3 is turned on. C_2 's stored energy begins to transfer the output. A branch D_2 , C_4 , and V_{out} make the flyback part, in which the energy that is transferred to the load by means of C_3 has turned positive and L_2 has become positive, and L_2 begins to charge the device. Capacitor C_1 consumes the energy stored in the leakage inductance, allowing voltage surges on the switch to be avoided, which is a key aspect of the proposed converter.

The inductor current i and output voltage can be written as follows:

$$\begin{aligned} \Delta i_{L1} &= \frac{V_{in}}{L_1}, \\ DT &= \frac{V_0 - 2V_{in}}{L_1} DT, \\ V_0 &= \frac{2-D}{1-D} V_{in}. \end{aligned} \quad (2)$$

3. Design Steps for Proposed Converters

The proposed converter duty cycle should be met for it to function properly. Otherwise, the super lift conversion will not be able to develop shoot-through circumstances, and the necessary voltage will not reach the load. The capacity of C_2 is critical to the correct functioning of the converter. In this case, the required value for C_2 is chosen such that the capacitor's discharging time interval is greater than $(1-D_2)T_s$. As a result, its voltage will not be negative or zero in this case. Otherwise, the output voltage is greatly reduced. The theoretical operating waveform of the proposed converter is shown in Figure 5. The magnetizing inductance is used to transport energy to the output node in the proposed converter.

The approach to evaluate the current and value of the magnetizing inductance is as follows:

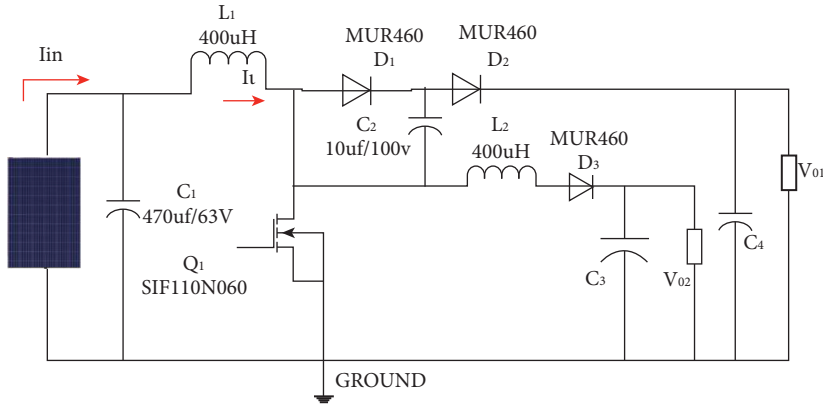


FIGURE 2: Circuit diagram of SIMO Converter. The operation of the converter can be given in two modes.

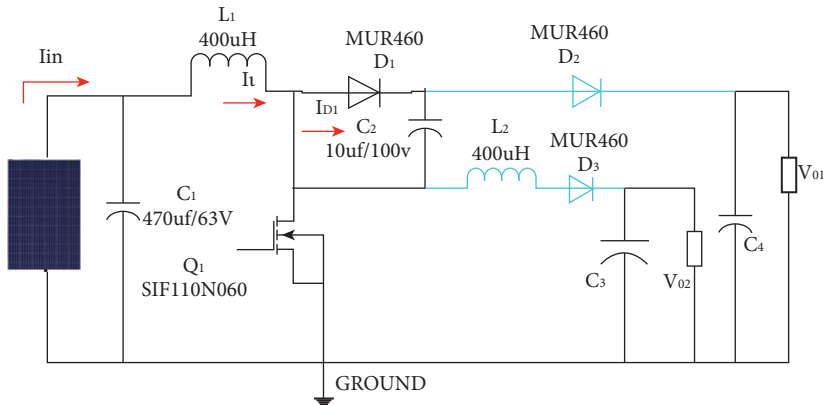


FIGURE 3: Mode 1 operation.

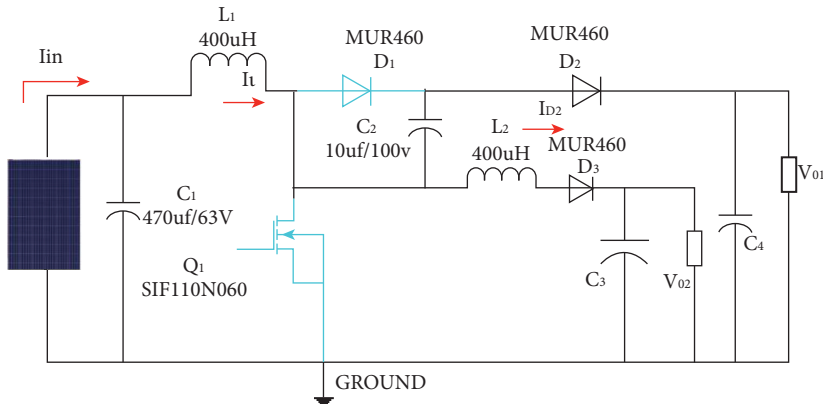


FIGURE 4: Mode 2 operation.

$$V_{L1} = L_1 \frac{\Delta i_{L1}}{\Delta t}, \quad (3)$$

$$L_1 = V_{in} \frac{d}{f \Delta i_{L1}}.$$

Switching current is determined by the converter's duty cycle at the lowest input voltage. The lowest input voltage determines the maximum switch current.

$$\% \text{Duty Cycle} = \frac{V_{in}(\text{min}) * \eta}{V_{out}}. \quad (4)$$

where η is the efficiency, which is assumed to be 80%, and V_{out} is the desired output voltage.

The average input current to the inductor is I_{L1} , and the inductor ripple current is given as ΔI_{L1} . If I_{L1} is present, it should be between 20% and 40%. The inductor current can be expressed as follows:

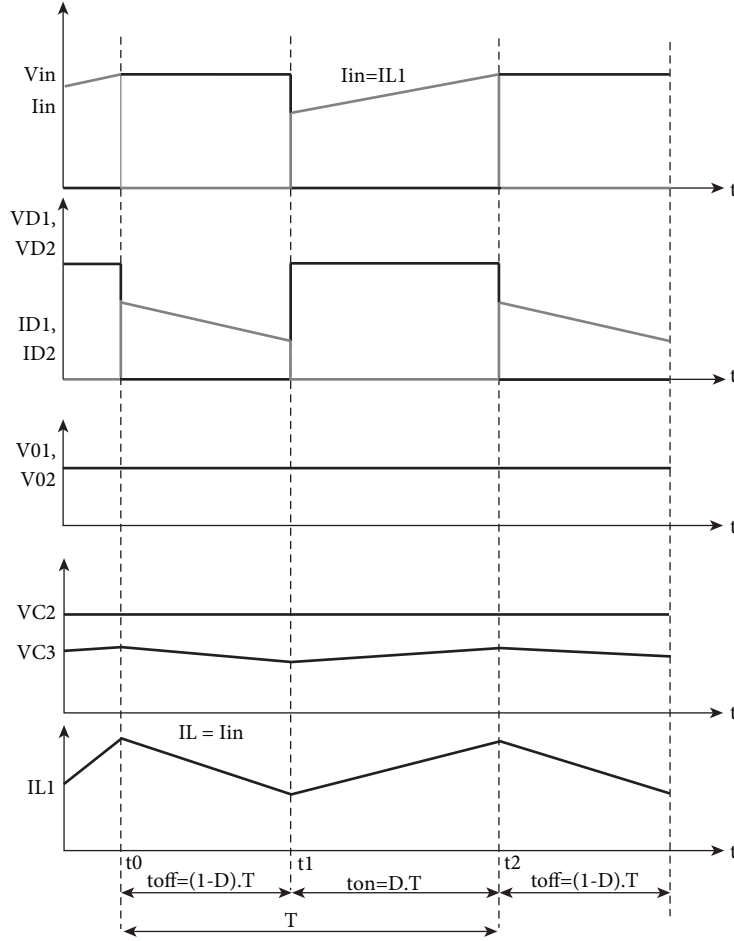


FIGURE 5: Theoretical operating waveform of proposed converter.

$$I_{L1} = \frac{V_{out}^* I_{out} (max)}{V_{in}^* \eta}, \quad (5)$$

$$I_{L1} = \frac{V_{in}^* (V_{out} + V_{d1} - V_{in})}{\Delta I_{L1}^* f_s^* (V_{out} + V_{d1})},$$

where V_{d1} is the forward voltage drop of the diode. Now, the inductor ripple current can be given as,

$$\Delta I_{L1} = \frac{V_{in} (min)^* Duty\ Cycle}{f_s^* L_1}. \quad (6)$$

The suitable value of C_2 is chosen based on two major modes and the capacitor's discharging intervals. Its expression is given by the following:

$$C_2 = I_{L1} \frac{d}{f \Delta i_{C2}}. \quad (7)$$

Output capacitors also have low equivalent series resistance (ESR). The equation of the capacitor C_3 can be given as follows:

$$C_3 = \frac{I_{out} (max)^* Duty\ Cycle}{f_s^* \Delta V_{out}}. \quad (8)$$

The output voltage oscillations should be monitored because of the influence of the capacitance voltage drop. The amp-sec equilibrium approach is used to find C_4 , and the change in output voltage can be written as follows:

$$C_4 = \frac{1-d}{f R_{02} (\Delta V_{02}/V_{02})}, \quad (9)$$

$$\Delta V_{01} = ESR^* \left(\frac{I_{out}}{1-D} + \frac{\Delta I L}{2} \right).$$

3.1. Voltage Gain. In establishing the converter, it is critical to choose the right L_m and duty cycle ratios. Conversion gains, losses, and fluctuations are among the design considerations. The voltage gains for the inductances are computed using ideal components and low fluctuations [24, 25]. The voltage gain of the SIMO converter is reported in this section, which is determined from the converter's

operation modes in the preceding section and depends on the voltage-second balancing of inductances. The voltage variation factor is computed by the volt-second equilibrium of the inductances. The voltage gain can be expressed as follows:

$$\begin{aligned} G_1 &= \frac{V_{01}}{V_{in}}, \\ &= \frac{2}{1-D}, \\ G_2 &= \frac{V_{02}}{V_{in}}, \\ &= \frac{1}{1-D}. \end{aligned} \quad (10)$$

3.2. Dynamic Modeling of the Proposed Converter. The voltages of the capacitors C_2 and C_3 and the current of inductors L_1 and L_2 are taken as state variables, and the state-space relations of the proposed converter can be written as follows:

$$\begin{aligned} \begin{bmatrix} \frac{di_{L1}}{dt} \\ \frac{di_{L2}}{dt} \\ \frac{dV_{C1}}{dt} \\ \frac{dV_{C2}}{dt} \end{bmatrix} &= \begin{bmatrix} \frac{-R_{01}}{L_1} & 0 & 0 & 0 \\ 0 & \frac{-R_{02}}{L_1} & \frac{1}{L_2} & \frac{-1}{L_2} \\ 0 & \frac{1}{C_2} & 0 & 0 \\ 0 & \frac{1}{C_3} & 0 & \frac{-1}{R_0 C_3} \end{bmatrix} \begin{bmatrix} i_{L1} \\ i_{L2} \\ V_{C2} \\ V_{C3} \end{bmatrix} + \begin{bmatrix} \frac{1}{L_1} \\ \frac{1}{L_2} \\ 0 \\ 0 \end{bmatrix} [V_{in}], \\ V_{C3} &= [0 \ 0 \ 0 \ 1] \begin{bmatrix} i_{L1} \\ i_{L2} \\ V_{C2} \\ V_{C3} \end{bmatrix}. \end{aligned} \quad (11)$$

State-space equations of the Luo converter when the switch Q_1 is turned off are represented as follows:

$$\begin{aligned} \begin{bmatrix} \frac{di_{L1}}{dt} \\ \frac{di_{L2}}{dt} \\ \frac{dV_{C1}}{dt} \\ \frac{dV_{C2}}{dt} \end{bmatrix} &= \begin{bmatrix} \frac{-R_{01}}{L_1} & 0 & \frac{-1}{L_1} & 0 \\ 0 & \frac{-R_{02}}{L_2} & 0 & \frac{-1}{L_2} \\ \frac{1}{C_2} & 0 & 0 & 0 \\ 0 & \frac{1}{C_2} & 0 & \frac{-1}{R_0 C_3} \end{bmatrix} \begin{bmatrix} i_{L1} \\ i_{L2} \\ V_{C2} \\ V_{C3} \end{bmatrix} + \begin{bmatrix} \frac{1}{L_1} \\ \frac{1}{L_2} \\ 0 \\ 0 \end{bmatrix} [V_{in}], \\ V_{C3} &= [0 \ 0 \ 0 \ 1] \begin{bmatrix} i_{L1} \\ i_{L2} \\ V_{C2} \\ V_{C3} \end{bmatrix}. \end{aligned} \quad (12)$$

3.3. Design of MPPT. The P&O approach is the most widely used MPPT technique for PV arrays. Perturb is a word that means “to revamp.” The PV module’s current or voltage is modified on a regular basis, and the output power is measured [26]. If an increase in power is linked to an increase in voltage, the control system will adjust the PV array’s operating temperature to the same position. This process is repeated until the maximum power point has been attained. The PV array’s working voltage is disturbed or modified a little, and the consequent change in power is estimated. If ΔP is high, then a rise in the PV panel’s voltage raises the PV array’s working point closer to the maximum power output. If ΔP is low, the operating temperature of the PV array is shifted further from the maximum output point.

4. Results and Discussion

The execution of the SIMO converter is discussed in this section. MATLAB/Simulink software was used to create and simulate the P&O MPPT approach. The PV panel’s specifications under standard operating conditions (STC) are utilized in this system. Table 1 shows the proposed converter’s design parameter values. Figure 6 shows the power output for a SIMO-based PV system utilizing the P&O approach. The P&O-based MPPT algorithm delivers significant power output in this system. The output power of P&O’s SIMO can produce up to 24 V, while the flyback converter provides 42 V. As a result, it is determined that combining a P&O-based MPPT with a SIMO converter for a PV system produces higher power outputs.

TABLE 1: Parameters of proposed converter.

Parameters	Symbol	Value
Input voltage	V_{input}	12 V
Output voltage	V_{o1}	24 V
	V_{o2}	48 V
Capacitor	C_2	470 μf
	C_3	660 μf
	C_4	440 μf
Inductor	L_1, L_2	400 μH
Switching frequency	Fs	42000 Hz
Input capacitor	C_{input}	200 μf

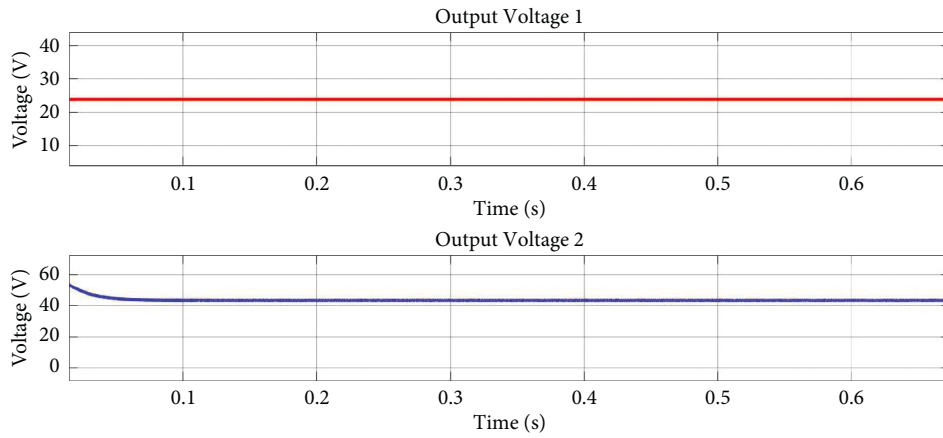


FIGURE 6: Simulation response of output voltages.

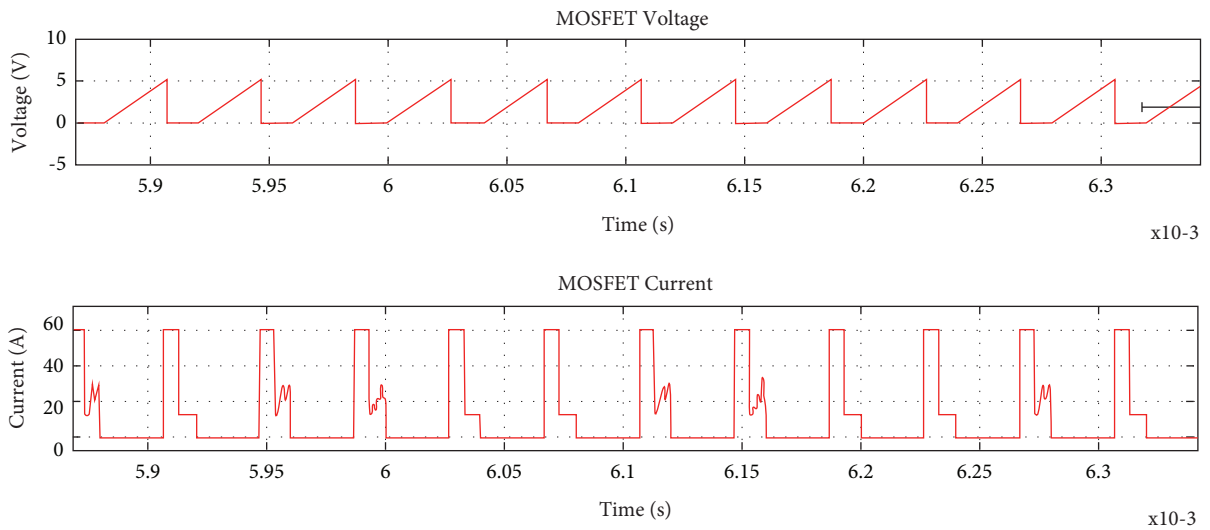
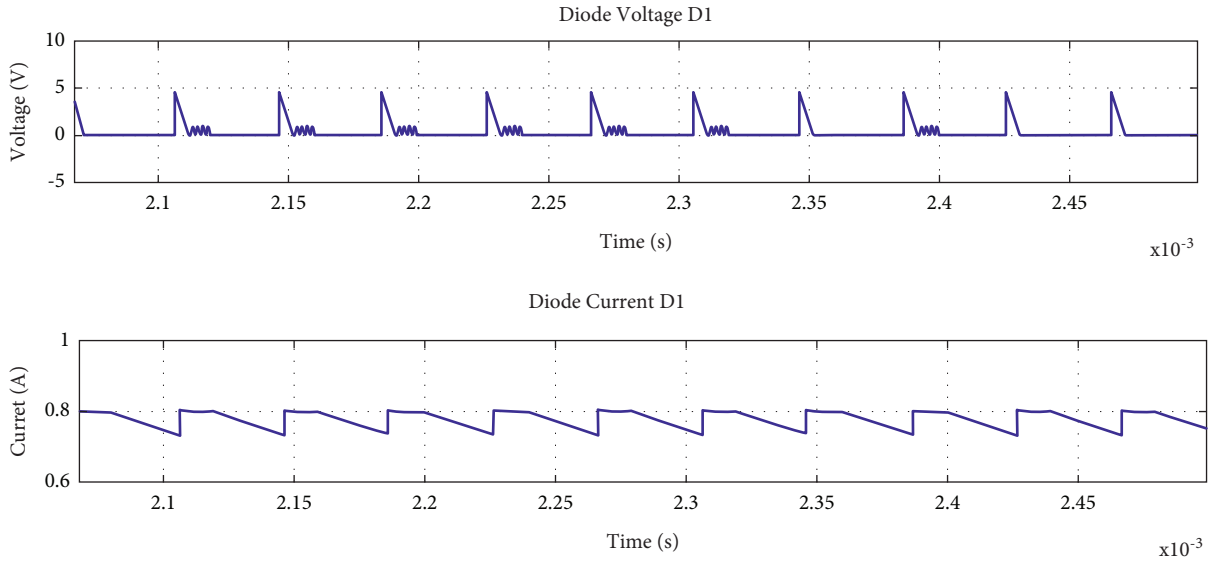
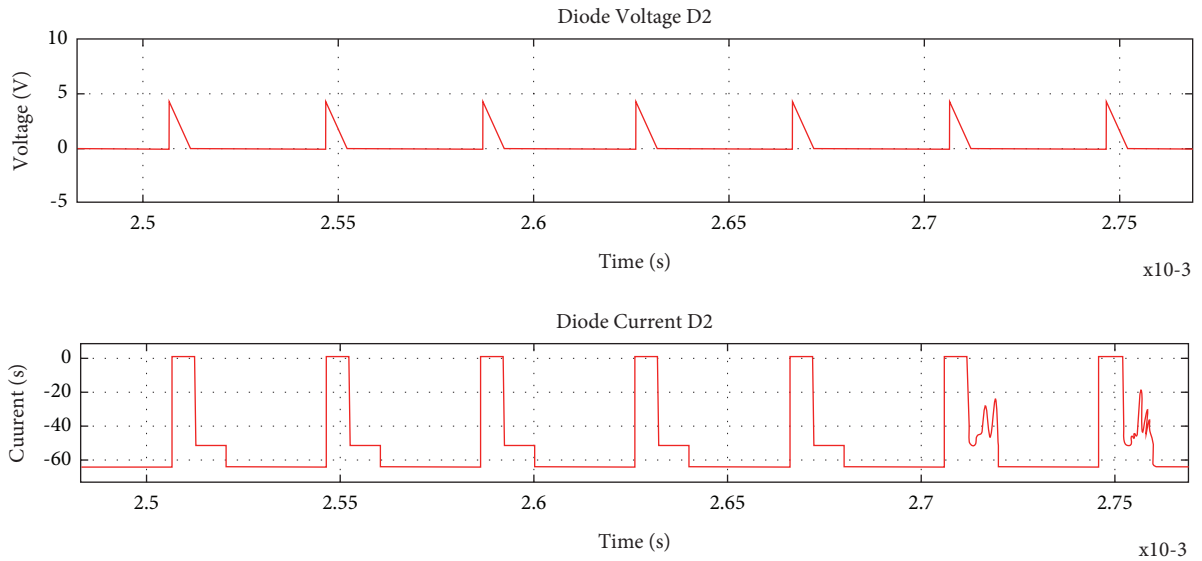


FIGURE 7: Simulation response of switching voltage and current.

The controlling MOSFET voltage and current waveforms are presented in Figure 7. As can be observed, the ripples of the input current can be reduced. The switch's switching voltage is 5 V. It demonstrates that during the ON state, the current through the inductor develops linearly and the diode prevents it. In pulse width modulation, the frequency stays unchanged, and the converter operates in two modes. When

the MOSFET switch is in mode 1, and the inductor 2 polarity is reversed in mode 2. The voltage and current waveform of diode D_1 are represented in Figure 8. During the turn-on switch Q_1 , the diode D_1 acts as a forward bias. During the turning time of switch Q_1 , the voltage across the diode is 5 V, and the current through the diode is 0.8 A. The voltage and current waveform of diode D_2 are represented in Figure 9.

FIGURE 8: Simulation response of diode D_1 voltage and current.FIGURE 9: Simulation response of diode D_2 voltage and current.

During the turn-on switch Q_1 , the diode D_2 acts as a reverse bias. After switching off Q_1 , the voltage across the diode is 5 V.

The inductor waveform is obtained by switching the inductor at a switching frequency of 42 kHz. The voltage and current waveforms of inductance and capacitance are illustrated in Figure 10. When a MOSFET is switched on, the input voltage V_{in} is supplied to the inductor network, and the current in the circuit attempts to climb while the coil is storing energy. During this period, the output capacitor supplies the load current. There is no voltage surge across the switch because the energy held in the leakage current is released

through the diodes D_1 and C_2 in the switch turn-off moment, which is a feature of the proposed converter that leads to minimal switching fatigue and capacitive turn-on loss. However, the proposed converter's Luo configuration reduces output ripple current and preserves efficiency at high voltage.

4.1. Experimental Validation. A 20 W CCM prototype was developed to validate the theoretical analysis. Figure 11 depicts the proposed converter's prototype. The proposed converter is linked to the control component of the MPPT method, which is accomplished using the STM32f103c6

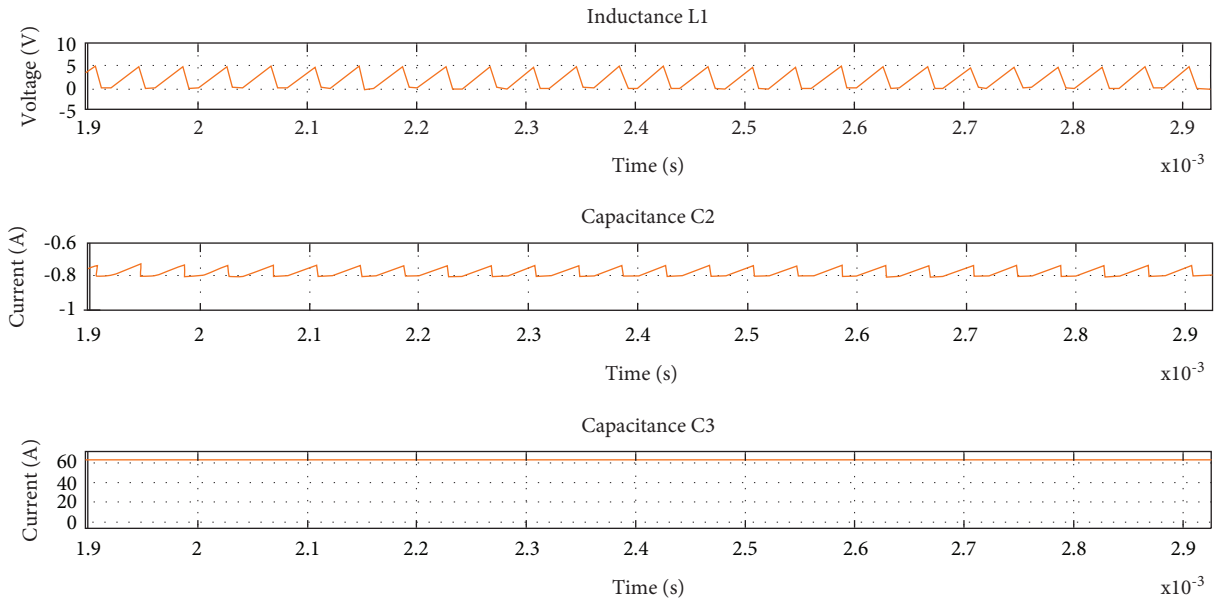


FIGURE 10: Simulation response of inductor and capacitor output.

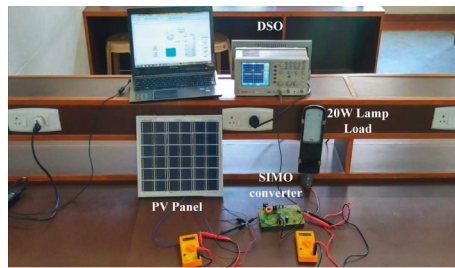


FIGURE 11: Experimental prototype of proposed converter.

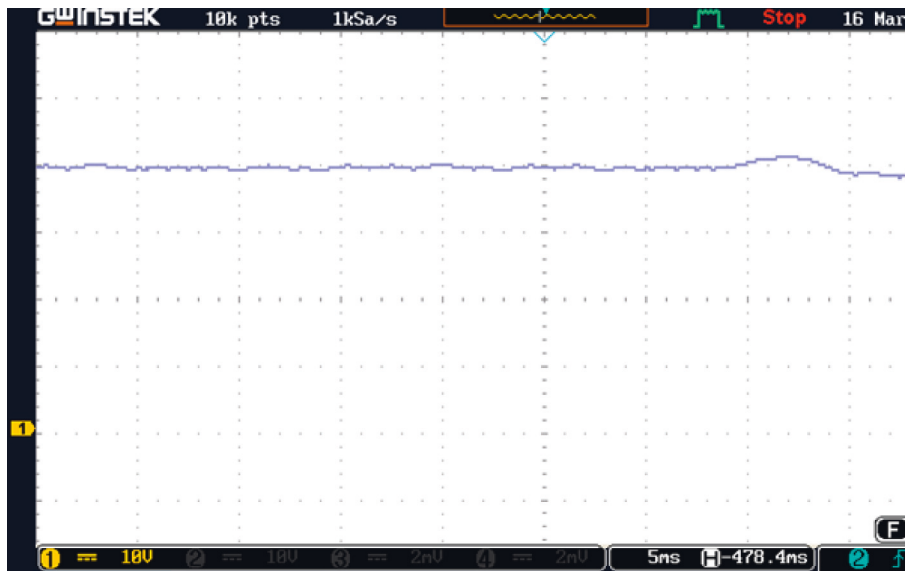
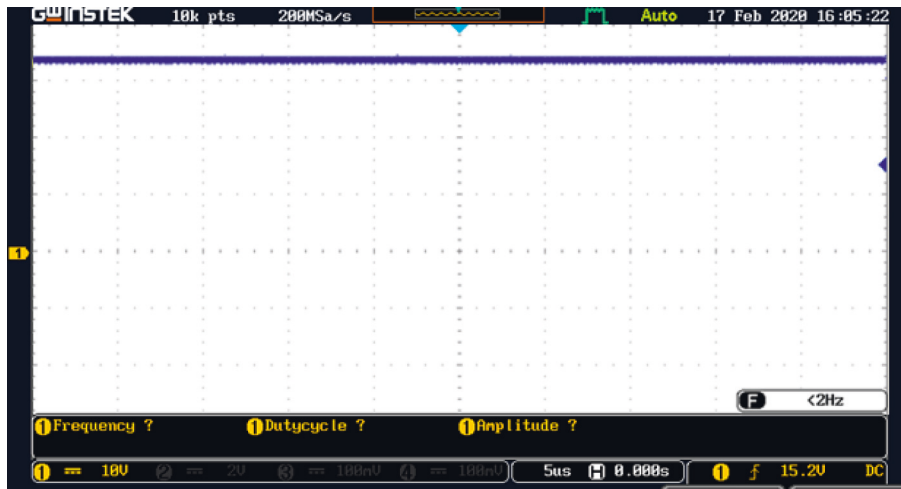
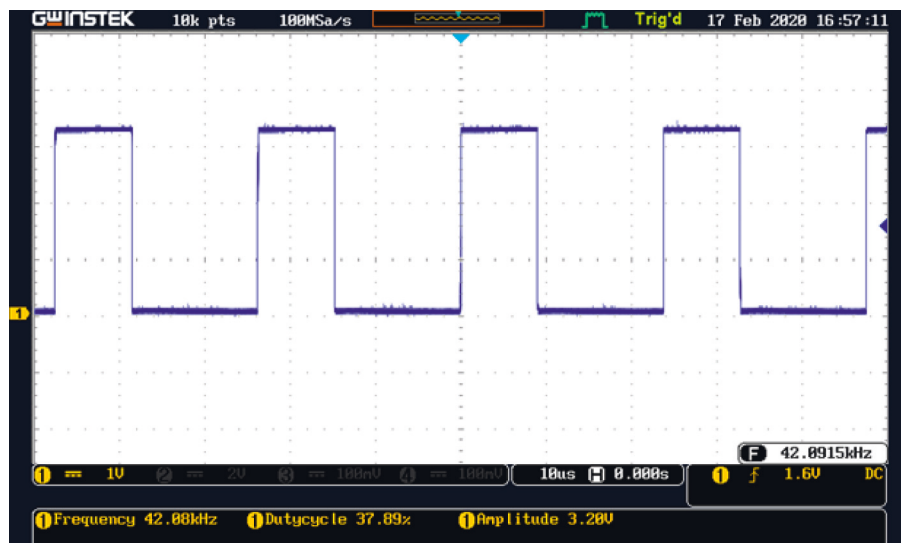
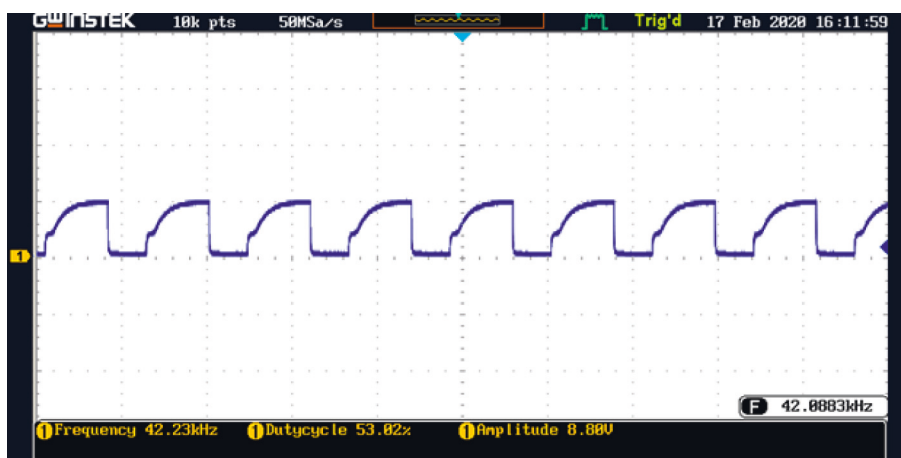


FIGURE 12: Experimental waveform of Output voltage V_{01} .

FIGURE 13: Experimental waveform of Output voltage V_{O2} .FIGURE 14: Experimental waveform of Switching Pulse to Q_1 .FIGURE 15: Experimental waveform of Voltage across V_{D1} .

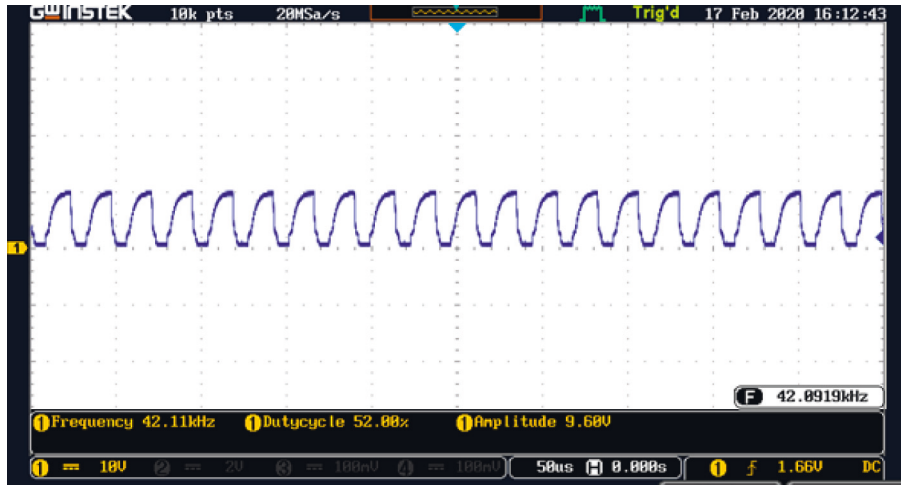
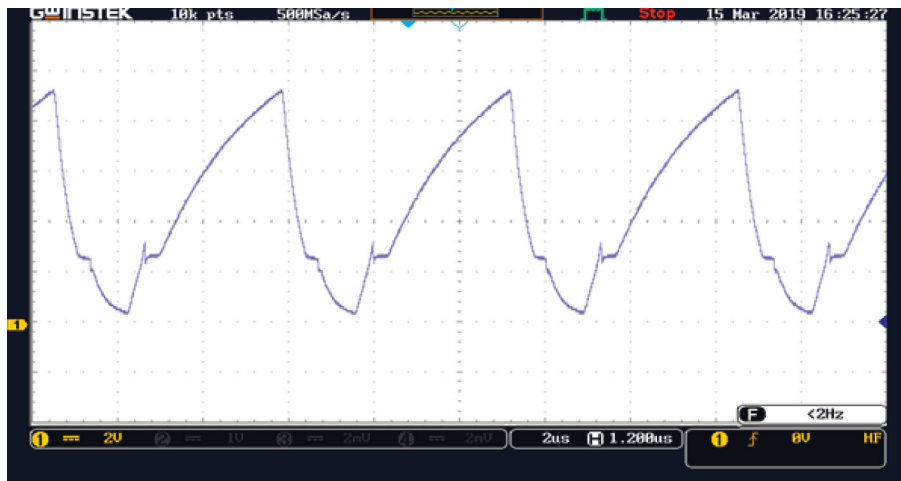
FIGURE 16: Experimental waveform of Voltage across V_{D2} .FIGURE 17: Experimental waveform of Voltage across V_{L1} .

TABLE 2: Comparison of proposed work with previous works.

References	Number of switches					G_1	G_2	Efficiency
	Switch	Capacitor	Diode	Inductor	Total outputs			
[1]	2	6	6	2	2	$(1/1 - D)$	$(2/1 - D)$	93.98
[2]	1	5	2	2	2	$((1 + N_2)/(1 - D)^2)$	$(2 + N_2/(1 - D)^2)$	93.4
[5]	3	7	4	1	2	$(2(N + 1))/D_1$	$(1 - D_3/D_1)$	92
[11]	1	3	4	2	1	$(1/1 - D_1)$	—	90
[23]	1	4	4	1	3	$(2 - D/1 - D)$	$(DN_b/1 - D)$	92.5
Proposed work	1	4	2	2	2	$(2/1 - D)$	$(1/1 - D)$	94.2

controller. The PV voltage and current are measured using a voltage and current sensor from the PV system. The detected signals are sent to the A/D interface, which converts the analogue signals to digital for the STM. The duty cycle is generated by multiplying the signal from the A/D port block by the gain value and feeding it to the MPPT section. The proposed converter is designed to behave with an input voltage of 12 V and output voltages of 24 V and 36 V. The output voltage of the converter's first port (1 Div = 10 Volt) is shown in Figure 12. The converter's output voltage is 24 volts

(1 Div = 10 volts). The output voltage of the converter's second port is seen in Figure 13. The voltage output of the converter's second port is 36 V (1 Div = 10 Volts). It shows that the output voltage is 3 times greater than the input voltage.

See Figure 14 shows the PWM output signal of a DSO waveform with a duty cycle of 37.89%. The Q_1 switch has a switch voltage of 3.2 V (1 Div = 1 V). It illustrates that during the ON state, inductor current L_1 develops linearly while the diode D_2 blocks it. When the MOSFET switch is switched off,

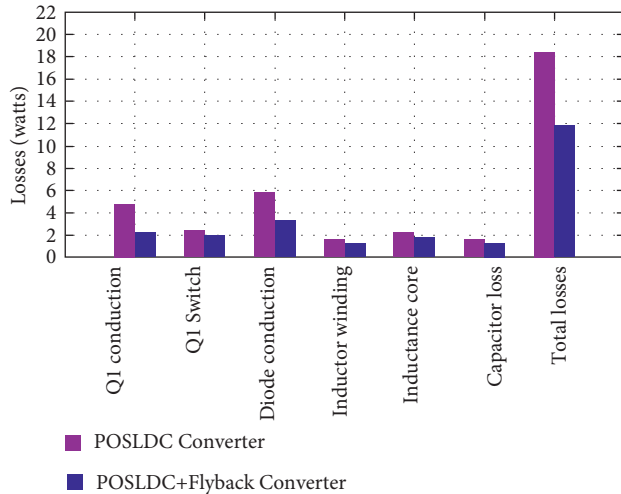


FIGURE 18: Comparison of the power losses of proposed converter with POSLDC Converter.

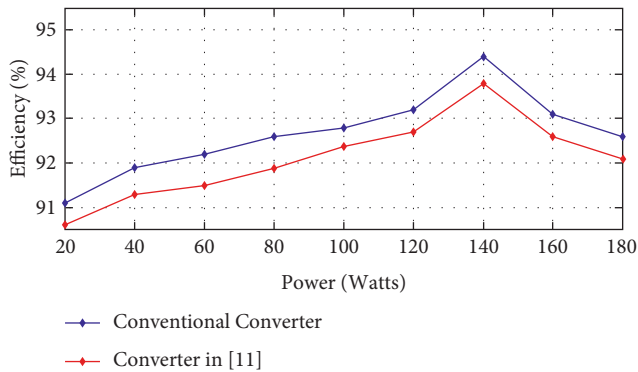


FIGURE 19: Efficiency vs. power graph of proposed converter with conventional converter.

no channel is formed between the drain and the source. As a result, the current flowing through the inductor L_1 does not change and begins to conduct, following the modulation process, and when energy is transferred from L_1 to D_2 , the current in the inductor L_1 decreases.

The experimental waveform of voltage across the diodes D_1 and D_2 is shown in Figures 15 and 16. The output voltages are lower than the voltages between the diodes D_1 and D_2 . The resonance interactions between stray inductance and the parasitic capacitance of diodes are mostly responsible for half-cycle fluctuations in the observed waveforms of V_{D1} and V_{D2} . Figure 17 depicts the waveform of inductive voltage. It has five voltage levels (1 Div = 2 V). It demonstrates that in pulse width modulation, the frequency stays unchanged, and the converter operates in two modes. When the MOSFET switch is in mode 1, the inductor polarity is reversed in mode 2. The voltage stress of the switches is found to be appropriate in proportion to the output voltages. Conduction loss becomes prominent because of the rapid current flow through the switch. As a consequence, high-power

semiconductors with minimal on-resistance values can be used to increase SIMO efficiency.

5. Discussion

There are numerous stepping techniques that can be chosen for SIMO converters. However, it is difficult to dispute that one SIMO is more powerful than the other. Table 2 compares the proposed SIMO converter's properties to those of similar earlier works. The collection can be formed using the number of switches, components, voltage gain, and efficiency as criteria. The proposed converter features a lower number of components on its single switch, a lower overall number of devices, and higher efficiency than previous SIMO converters. Figure 18 depicts the experimental findings of the converter efficiency under various load circumstances. The converter efficiency is anticipated to be 94.2% at full load power. Figure 19 compares the efficiency of the proposed converter to that of a POSLDC converter, with a predicted total loss variation of 6.45 W. The bulk of the efficiency difference between the two converters is because of lower conduction losses.

6. Conclusion

In this paper, a SIMO converter with Luo network integration has been developed for EV. A simulation was performed in MATLAB/SIMULINK to study the proposed converter's operational principles, and an experimental setup was built in the laboratory to confirm the results. The proposed converter has various benefits over typical converters, such as efficient high voltage gain and low losses across the switching than the output voltage. Furthermore, this proposed converter family can seamlessly integrate to obtain higher efficiency and compact size and can serve as enticing examples for new converter development in EV applications. Based on the power acquired, the proposed converter achieved 94.2% efficiency. In addition, as compared to a traditional converter, the power losses of 6.45 watts are minimized. Future studies will focus on investigating the circuit's bidirectional functioning, extending its operation to high voltages and improving its dynamical behavior.

Data Availability

Data will be available on request. For data-related queries, kindly contact Baseem Khan via baseem_khan04@yahoo.com.

Conflicts of Interest

The authors declare that they have no conflicts of interest.

References

- [1] I. A. Aden, H. Kahveci, and M. E. Şahin, "Design and implementation of single-input multiple-output DC-DC buck converter for electric vehicles," *Journal of Circuits, Systems, and Computers*, vol. 30, no. 13, 2021.

- [2] D. Yu, J. Yang, R. Xu, Z. Xia, H. H.-C. Iu, and T. Fernando, "A family of module-integrated high step-up converters with dual coupled inductors," *IEEE Access*, vol. 6, pp. 16256–16266, 2018.
- [3] R. A. Verzijlbergh, L. J. De Vries, and Z. Lukszo, "Renewable energy sources and responsive demand. do we need congestion management in the distribution grid?" *IEEE Transactions on Power Systems*, vol. 29, no. 5, pp. 2119–2128, 2014.
- [4] M. Z. Malik, H. Chen, M. S. Nazir et al., "A new efficient step-up boost converter with CLD cell for electric vehicle and New Energy Systems," *Energies*, vol. 13, no. 7, p. 1791, 2020.
- [5] S. Song, G. Chen, Y. Liu, Y. Hu, K. Ni, and Y. Wang, "A three-switch-based single-input dual-output converter with simultaneous boost & buck voltage conversion," *IEEE Transactions on Industrial Informatics*, vol. 16, no. 7, pp. 4468–4477, 2020.
- [6] C. Wang, M. Li, Z. Ouyang, and G. Wang, "Resonant push-pull converter with flyback regulator for mhz high step-up power conversion," *IEEE Transactions on Industrial Electronics*, vol. 68, no. 2, pp. 1178–1187, 2021.
- [7] N. Mohammadian and M. R. Yazdani, "Half-bridge flyback converter with lossless passive snubber and interleaved technique," *IET Power Electronics*, vol. 11, no. 2, pp. 239–245, 2018.
- [8] K. C. Tseng, H. S. Huang, and C. A. Cheng, "Integrated boost-forward-flyback converter with high step-up for Green Energy power-conversion applications," *IET Power Electronics*, vol. 14, no. 1, pp. 27–37, 2020.
- [9] R.-J. Wai and K.-H. Jheng, "High-efficiency single-input multiple-output DC-DC converter," *IEEE Transactions on Power Electronics*, vol. 28, no. 2, pp. 886–898, 2013.
- [10] P. Patra, A. Patra, and N. Misra, "A single-inductor multiple-output switcher with simultaneous Buck, boost, and inverted outputs," *IEEE Transactions on Power Electronics*, vol. 27, no. 4, pp. 1936–1951, 2012.
- [11] S. Saravanan and N. R. Babu, "Design and development of single switch high step-up DC-DC converter," *IEEE Journal of Emerging and Selected Topics in Power Electronics*, vol. 6, no. 2, pp. 855–863, 2018.
- [12] S. K. Mishra, K. K. Nayak, M. S. Rana, and V. Dharmarajan, "Switched-boost action based multiport converter," *IEEE Transactions on Industry Applications*, vol. 55, no. 1, pp. 964–975, 2019.
- [13] Z. Saadatizadeh, P. C. Heris, E. Babaei, and M. Sabahi, "A new nonisolated single-input three-output high voltage gain converter with low voltage stresses on switches and diodes," *IEEE Transactions on Industrial Electronics*, vol. 66, no. 6, pp. 4308–4318, 2019.
- [14] S. K. Ramu, S. Paramasivam, S. Muthusamy, H. Panchal, K. K. Sadasivuni, and Y. Noorollahi, "A novel design of switched boost action based multiport converter using dsPIC controller for Renewable Energy Applications," *Energy Sources, Part A: Recovery, Utilization, and Environmental Effects*, vol. 44, no. 1, pp. 75–90, 2021.
- [15] J. Gupta and B. Singh, "Bridgeless isolated positive output Luo converter based high power factor single stage charging solution for Light Electric Vehicles," *IEEE Transactions on Industry Applications*, vol. 58, no. 1, pp. 732–741, 2022.
- [16] E. Gerami, M. Delshad, M. R. Amini, and M. R. Yazdani, "A new family of non-isolated PWM DC-DC converter with soft switching," *IET Power Electronics*, vol. 12, no. 2, pp. 237–244, 2019.
- [17] G. K. Srinivasan, H. T. Srinivasan, and M. Rivera, "Low-cost implementation of passivity-based control and estimation of load torque for a Luo converter with dynamic load," *Electronics*, vol. 9, no. 11, p. 1914, 2020.
- [18] A. T. Mohammed and N. K. Alshamaa, "Design and implementation of a modified Luo converter with higher-voltage ratio gain," *IOP Conference Series: Materials Science and Engineering*, vol. 881, no. 1, Article ID 012124, 2020.
- [19] B. Singh and R. Kushwaha, "Power factor preregulation in interleaved Luo Converter-fed electric vehicle battery charger," *IEEE Transactions on Industry Applications*, vol. 57, no. 3, pp. 2870–2882, 2021.
- [20] R. Shenbagalakshmi, K. Geetha, and S. Vijayalakshmi, "Design and analysis of discrete PID controller for Luo Converter," *International Journal of Power Electronics*, vol. 11, no. 3, p. 283, 2020.
- [21] F. L. Luo and H. Ye, *Super-lift Converters and Ultra-lift Converters*, pp. 377–516, Renewable Energy Systems, 2017.
- [22] S. Saravanan and N. Ramesh Babu, "Maximum power point tracking algorithms for Photovoltaic System-a Review," *Renewable and Sustainable Energy Reviews*, vol. 57, pp. 192–204, 2016.
- [23] F. Ghasemi, M. R. Yazdani, and M. Delshad, "Step-up DC-DC switching converter with single switch and multi-outputs based on Luo Topology," *IEEE Access*, vol. 10, pp. 16871–16882, 2022.
- [24] M. Mahdavi, M. Shahriari-kahkeshi, and N. R. Abjadi, "An adaptive estimator-based sliding mode control scheme for uncertain POESLL converter," *IEEE Transactions on Aerospace and Electronic Systems*, vol. 55, no. 6, pp. 3551–3560, 2019.
- [25] B. Akhlaghi, N. Molavi, M. Fekri, and H. Farzanehfard, "High step-up interleaved ZVT converter with low voltage stress and automatic current sharing," *IEEE Transactions on Industrial Electronics*, vol. 65, no. 1, pp. 291–299, 2018.
- [26] S. Saravanan and N. Ramesh Babu, "RBFN based MPPT algorithm for PV system with high step up converter," *Energy Conversion and Management*, vol. 122, pp. 239–251, 2016.